

# Numerical computation of the beta function of large $N$ $SU(N)$ gauge theory coupled to an adjoint Dirac fermion

A. Hietanen\*

*CP3-Origins and the Danish Institute for Advanced Study DIAS,  
University of Southern Denmark, Campusvej 55, DK-5230 Odense M, Denmark.*

R. Narayanan†

*Department of Physics, Florida International University, Miami, FL 33199, USA.*

(Dated: June 15, 2021)

We use a single site lattice in four dimensions to study the scaling of large  $N$  Yang-Mills field coupled to a single massless Dirac fermion in the adjoint representation. We use the location of the strong to weak coupling transition defined through the eigenvalues of the folded Wilson loop operator to set a scale. We do not observe perturbative scaling in the region studied in this paper. Instead, we observe that the scale changes very slowly with the bare coupling. The lowest eigenvalue of the overlap Dirac operator is another scale that shows similar behavior as a function of the lattice coupling. We speculate that this behavior is due to the beta function approaching close to a zero.

PACS numbers: 12.20.-m

Keywords:  $1/N$  Expansion, Adjoint fermions, Lattice Gauge Field Theories, Conformal Field Theories, Infrared Fixed Points

## I. INTRODUCTION

Particle accelerators experiments provide strict bounds for the beyond standard model physics. For technicolor it means that the coupling constant has to exhibit walking behavior. Otherwise the theory cannot simultaneously explain the mass pattern of standard model fermions and the suppression of the flavor changing neutral currents [1–4]. Hence, lattice studies of vector like gauge theories with appropriate choice of fermion matter with the aim of understanding the conformal window has recently attracted considerable attention (see [5] and references therein). The gauge group is chosen to be  $SU(N)$  and the number and representation of fermions is such that the theory is expected to be conformal or near conformal [6].

Let

$$b = \frac{1}{g^2 N} \quad (1)$$

define the inverse 't Hooft coupling on the lattice. Let

$$t = \ln a \quad (2)$$

define the logarithm of a lattice scale where  $a(b)$  could be the square root of the string tension measured on the lattice at the coupling  $b$ . The beta function of the lattice is defined as

$$\beta(b) = \frac{db(t)}{dt}. \quad (3)$$

The perturbative beta function leads off as

$$\beta(b) = -b_0 - \frac{b_1}{b} + \dots \quad (4)$$

As is well known [7], only the one and two loop coefficients,  $b_0$  and  $b_1$ , are universal and the higher order coefficients in a Taylor expansion of  $\beta(b)$  in powers of  $b^{-1}$  depend on the choice of  $a(b)$ . In fact, one can imagine choosing an

---

\*Electronic address: hietanen@cp3-origins.net

†Electronic address: rajamani.narayanan@fiu.edu

$a(b)$  such that all higher order coefficients are zero. We will not have such control on the choice of  $a(b)$ . In particular, there is no reason to expect the location of the zero of the beta function to be independent of the choice of  $a(b)$  – all we can expect is for the zero to remain stable if it is at a perturbatively weak coupling.

The choice of fermionic matter can be motivated by the presence of a zero in the two-loop perturbative beta function. In order to maintain asymptotic freedom, all choices are such that  $b_0 > 0$ . The two loop beta function has a zero if  $b_1 < 0$ . Some of the choices currently being investigated are:

- SU(3) gauge group with twelve Dirac flavors of fermions in the fundamental representation [8–10] –  $b_1$  is negative if we have nine or more Dirac flavors but the zero of the two loop beta function occurs at smaller coupling for larger flavors.
- SU(2) gauge group with two Dirac flavors of fermions in the adjoint representation [11–14] – This is the only choice based upon  $b_0$  and  $b_1$  since  $b_0 < 0$  if we choose three or more Dirac flavors and  $b_1 > 0$  if we choose one Dirac flavor.
- SU(3) gauge group with two Dirac flavors in the two-index symmetric representation [15–17] – In this case  $b_1 > 0$  if there is only one Dirac flavor. One can also choose three Dirac flavors and still maintain asymptotic freedom.

The case of SU( $N$ ) gauge theory coupled to  $f$  flavors of Dirac fermions in the adjoint representation is interesting for two reasons:

- The first two coefficients of the beta function are

$$b_0 = \frac{11 - 4f}{24\pi^2}; \quad b_1 = \frac{17 - 16f}{192\pi^4}, \quad (5)$$

and are independent of  $N$  [33]. The three interesting choices for a theory with an infra-red fixed point are  $f = \frac{3}{2}, 2, \frac{5}{2}$  based on the two-loop beta function.

- Numerical evidence along with continuum arguments [18]–[26] suggest that Eguchi-Kawai reduction holds in the large  $N$  limit as long as one uses periodic boundary conditions for fermions. This is expected to be the case for  $f \geq \frac{1}{2}$  [22] and for non-zero quark masses [19].

We have the possibility to study theories with an infra-red fixed point that have only four  $SU(N)$  degrees of freedom provided we consider the  $N \rightarrow \infty$  limit. For finite  $N$ , the massless fermionic operator is a finite dimensional operator that decouples into chiral sectors. The fermion determinant is positive in each chiral sector and we can define a theory for any real value  $f$  since we can write

$$(\det \not{D})^f = e^{f \ln \det \not{D}}. \quad (6)$$

If  $\frac{11}{4} > f > \frac{17}{16}$ , the two loop beta function has a zero and the theory has an infra-red fixed point.

Our aim in this paper is to use overlap fermions [28]–[30] and study the  $f = 1$  theory on a single site lattice. We do not expect the beta function to have a zero from the perturbative viewpoint. Even if it has a zero, we expect it to be at strong coupling. With this in mind we expect a computation of the running coupling to agree with the two-loop running. Contrary to this expectation, we will show that the coupling runs much faster than what is expected from perturbative running.

The model on the single site lattice is defined in Sec. II. We will numerically study this model using the Hybrid Monte Carlo (HMC) algorithm with pseudofermions as described in Sec. III. It is numerically difficult to extract the string tension. On the other hand there is an observable based on the Wilson loop operator [31, 32] that shows a transition from weak to strong coupling and we will use the location of this transition to set our scale as discussed in Sec. IV A. We will also look at the eigenvalues closest to zero of the overlap Dirac operator. We will compare the behavior of the lowest positive eigenvalue as a function of the lattice coupling and compare its behavior to the scale set using the Wilson loop operator.

Results for the behavior of the scales set using the Wilson loop operator and the lowest positive eigenvalue of the massless Dirac operator are discussed in detail for the case of theory with massless fermions in Sec. V. We will show that both scales are monotonic in the coupling and that they both vary very slowly with the coupling. We will speculate on the possibility of a near-zero of the beta function in Sec. VI.

## II. THE MODEL

The action on a single site lattice with one flavor of adjoint Dirac overlap fermion is given by

$$S = S_g + S_f. \quad (7)$$

The gauge action is

$$S_g = -12bNP; \quad P = \frac{1}{12} \sum_{\mu \neq \nu=1}^4 \text{Tr} [U_\mu U_\nu U_\mu^\dagger U_\nu^\dagger], \quad (8)$$

where the four gauge degrees of freedom,  $U_\mu$  ( $\mu = 1, 2, 3, 4$ ), are  $\text{SU}(N)$  matrices. The lattice gauge coupling constant is  $b = \frac{1}{g^2 N}$ . The overlap fermion action is

$$S_f = -f \ln \det H_o(\mu), \quad (9)$$

where the Hermitian massive overlap Dirac operator is defined by

$$H_o(\mu) = \frac{1}{2} [(1 + \mu) \gamma_5 + (1 - \mu) \epsilon(H)], \quad (10)$$

with  $\mu \in [0, 1]$  being the bare mass. We note that the eigenvalues of  $H_o(0)$  are in the range  $[-1, 1]$  with exact zero eigenvalues and exact  $\pm 1$  eigenvalues corresponding to a gauge background with non-zero topology. The Hermitian Wilson Dirac operator for adjoint fermions is given by

$$\begin{aligned} H &= \begin{pmatrix} 4 - m - \frac{1}{2} \sum_\mu (V_\mu + V_\mu^t) & \frac{1}{2} \sum_\mu \sigma_\mu (V_\mu - V_\mu^t) \\ -\frac{1}{2} \sum_\mu \sigma_\mu^\dagger (V_\mu - V_\mu^t) & -4 + m + \frac{1}{2} \sum_\mu (V_\mu + V_\mu^t) \end{pmatrix} \\ &= (4 - m) \gamma_5 - \sum_\mu (w_\mu V_\mu + w_\mu^\dagger V_\mu^t), \end{aligned} \quad (11)$$

where

$$w_\mu = \frac{1}{2} \begin{pmatrix} 1 & -\sigma_\mu \\ \sigma_\mu^\dagger & -1 \end{pmatrix} \quad (12)$$

and  $V_\mu$  are the link matrices in adjoint representation. The action of  $V_\mu$  on  $\Phi$  is given by

$$V_\mu \Phi = U_\mu \Phi U_\mu^\dagger; \quad V_\mu^t \Phi = U_\mu^\dagger \Phi U_\mu. \quad (13)$$

One can verify that  $H$  is Hermitian in the usual sense:

$$\text{Tr} \Psi^\dagger H \Phi = [\text{Tr} \Phi^\dagger H \Psi]^* = \text{Tr} [(H \Psi)^\dagger \Phi]. \quad (14)$$

Therefore  $\Psi^\dagger H = (H \Psi)^\dagger$  and in addition it is also true that  $\text{Tr} H \Phi = 0$  if  $\text{Tr} \Phi = 0$ . The same is also true for  $H_o(\mu)$ .

## III. THE NUMERICAL ALGORITHM

We used the Hybrid Monte Carlo (HMC) algorithm to generate  $U_\mu$  according to the measure

$$Z = \int [dU_\mu] e^{-S}. \quad (15)$$

Let us introduce a Hamiltonian

$$\mathcal{H} = \frac{1}{2} \sum_{\mu=1}^4 \text{Tr} H_\mu^2 + S, \quad (16)$$

where matrices,  $H_\mu$ ;  $\mu = 1, 2, 3, 4$  are elements of the  $su(N)$  algebra and conjugate to  $U_\mu$ . The HMC algorithm involves the computation of the force,  $\frac{\partial S}{\partial U_\mu^{ij}}$ . The gauge part of the force is simple to compute numerically, but the

fermionic part of the force is computationally intensive. An *exact* algorithm was developed in [22] to compute the fermionic part of the force. This algorithm scales like  $N^6$ . In addition to using this algorithm, we also developed a pseudo-fermion algorithm in order to compute the fermionic part of the force which scales like  $N^4$ . We present the details of the pseudo-fermion algorithm in this section. Both algorithms were used to obtain the numerical data presented in this paper.

We note that

$$H_{o\pm}^2(\mu) = \frac{1+\mu^2}{2}P_{\pm} \pm \frac{1-\mu^2}{2}P_{\pm}\epsilon(H)P_{\pm}; \quad P_{\pm} = \frac{1 \pm \gamma_5}{2}, \quad (17)$$

and

$$\det H_o(\mu) = \det H_{o+}^2(\mu) = \det H_{o-}^2(\mu), \quad (18)$$

in the zero topological sector. [34] The overlap fermion action can be rewritten as

$$S_f = \text{Tr} \left[ \Phi_+^\dagger [H_{o+}^2(\mu)]^{-1} \Phi_+ \right]; \quad (19)$$

where the pseudofermions  $\Phi_+$  have positive chirality and are traceless  $N \times N$  complex matrices with an additional two component spin index.

For numerical purposes, we will represent  $\epsilon(H)$  as

$$\epsilon(H) = \sum_{k=1}^n \frac{r_k H}{H^2 + p_k}; \quad 0 < p_1 < p_2 < \dots < p_n, \quad (20)$$

with  $n$  chosen such that the representation is accurate in the spectral range of  $H^2$  assuming some lower bound on the spectrum of  $H^2$ .

The algorithm starts with one choice for  $U_\mu$ . Then, we draw  $H_\mu$  according to a Gaussian distribution. We also draw Dirac indexed traceless Hermitian matrices,  $\Psi$  according to the Gaussian distribution,  $\text{Tr} \Psi^\dagger \Psi$ , and set

$$\Phi_+ = P_+ H_o(\mu) \Psi. \quad (21)$$

The equations of motion for  $U_\mu$  are

$$\frac{dU_\mu}{d\tau} = iH_\mu U_\mu. \quad (22)$$

Setting  $\frac{d\mathcal{H}}{d\tau} = 0$  results in

$$\sum_{\mu=1}^4 \text{Tr} \left[ H_\mu \frac{dH_\mu}{d\tau} \right] + \frac{dS_g}{d\tau} + \frac{dS_f}{d\tau} = 0, \quad (23)$$

and

$$\frac{dS_g}{d\tau} = \sum_{\mu=1}^4 \text{Tr} [H_\mu D_\mu^g]; \quad \frac{dS_f}{d\tau} = \sum_{\mu=1}^4 \text{Tr} [H_\mu D_\mu^f]. \quad (24)$$

The equation of motion for  $H_\mu$  is given by

$$\frac{dH_\mu}{d\tau} = -D_\mu^g - D_\mu^f. \quad (25)$$

Taking the derivative of  $S_g$  in (8) with respect to  $\tau$  and using (22) we arrive at

$$D_\mu^g = -ibN \sum_{\nu=1}^4 [U_\mu U_\nu U_\mu^\dagger U_\nu^\dagger + U_\mu U_\nu^\dagger U_\mu^\dagger U_\nu - U_\nu^\dagger U_\mu U_\nu U_\mu^\dagger - U_\nu U_\mu U_\nu^\dagger U_\mu^\dagger] \quad (26)$$

The derivative of  $S_f$  in (19) with respect to  $\tau$  using (17) is

$$\frac{dS_f}{d\tau} = -\frac{1-\mu^2}{2} \text{Tr} \left[ \Upsilon_+^\dagger \frac{d\epsilon(H)}{d\tau} \Upsilon_+ \right]; \quad \Upsilon_+ = [H_{o+}^2(\mu)]^{-1} \Phi_+. \quad (27)$$

Substituting the representation (20) for  $\epsilon(H)$ , we can write

$$\frac{dS_f}{d\tau} = -\frac{1-\mu^2}{2} \sum_{k=1}^n \left( r_k p_k \text{Tr} \left[ \Upsilon_k^\dagger \frac{dH}{d\tau} \Upsilon_k \right] - r_k \text{Tr} \left[ \Xi_k^\dagger \frac{dH}{d\tau} \Xi_k \right] \right); \quad (28)$$

where

$$\Upsilon_k = \frac{1}{H^2 + p_k} \Upsilon_+; \quad \Xi_k = H \Upsilon_k. \quad (29)$$

Using (11), (13) and (22), we can show that

$$\text{Tr} \left[ X^\dagger \frac{dH}{d\tau} X \right] = \sum_{\mu=1}^4 \text{Tr} [H_\mu A_\mu(X)], \quad (30)$$

where

$$A_\mu(X) = i \sum_{i,j=1}^4 \left( w_\mu^{\dagger ij} \left[ X_j, U_\mu X_i^\dagger U_\mu^\dagger \right] + w_\mu^{ij} \left[ X_i^\dagger, U_\mu X_j U_\mu^\dagger \right] \right), \quad (31)$$

for any complex matrix  $X$ . It is clear that  $A_\mu^\dagger(X) = A_\mu(X)$  and that  $\text{Tr} A_\mu(X) = 0$ . Therefore,

$$D_\mu^f = -\frac{1-\mu^2}{2} \sum_{k=1}^n [r_k p_k A_\mu(\Upsilon_k) - r_k A_\mu(\Xi_k)]. \quad (32)$$

Given  $\Phi_+$  in (21), we compute  $\Upsilon_+$  in (27) with the standard conjugate gradient algorithm. Each action of  $H_{o+}^2(\mu)$  that is part of the conjugate gradient algorithm involves the action of  $\epsilon(H)$  on a Dirac indexed traceless Hermitian matrix. We use the multiple mass conjugate algorithm for each action of  $\epsilon(H)$  represented by (20). The core of the fermion algorithm is the action of  $H$  on a Dirac indexed traceless Hermitian matrix and this operation scales like  $N^3$  [see (13)]. In addition, the computational cost depends on the gap of  $H$  and  $H_{o+}(\mu)$ . The former is large and therefore does not seriously affect the computational cost. Since we are interested in studying chiral properties of the theory and want to work with as small a bare mass,  $\mu$ , as possible the smallest eigenvalues of  $H_{o+}(0)$  will scale like  $N^{-2}$  and the condition number grows like  $N^2$ .

#### IV. OPERATORS

We will focus on measuring two quantities that will help us understand the running of the coupling with the scale and reveal numerical evidence for a singular point. One observable looks at the property of the gauge field and the other looks at the property of the massless fermion.

##### A. Weak to strong coupling transition [32]

A folded  $L \times L$  square Wilson loop operator in the  $\mu - \nu$  plane is given by

$$W(L) = U_\mu^L U_\nu^L U_\mu^\dagger U_\nu^\dagger. \quad (33)$$

The eigenvalues,  $e^{i\theta_k}$ ;  $k = 1, \dots, N$  of this operator are gauge invariant. Let  $p(\theta; L, b)$  be the distribution of these eigenvalues with  $\theta \in [-\pi, \pi)$ . This distribution undergoes a transition at  $N \rightarrow \infty$  as the size,  $L$ , is changed at a fixed coupling  $b$ : the distribution has a gap at  $\pi$  for small areas and it becomes gapless for areas larger than a critical area  $A_c(b)$ . There is a universal function describing the distribution in terms of the scaled variables derived from  $A(b)$  and  $\theta$  in the vicinity of  $A_c(b)$  and  $\pi$ .

Let

$$O_N(\xi; L, b) = \left\langle \det \left( e^{\frac{y}{2}} + e^{-\frac{y}{2}} W(L) \right) \right\rangle; \quad \xi = \tanh \frac{y}{2}. \quad (34)$$

The region close to  $\xi = 0$  probes  $\theta$  close to  $\pi$ . Let

$$O_N(\xi; L, b) = C_0(L, b, N) + C_1(L, b, N)\xi^2 + C_2(L, b, N)\xi^4 + \dots \quad (35)$$

It is useful to define a Binder cumulant type quantity

$$\Omega(L, b, N) = \frac{C_0(L, b, N)C_2(L, b, N)}{C_1^2(L, b, N)}. \quad (36)$$

One can show using the universal scaling function that

$$\Omega(L_c(b), b, \infty) = \frac{\Gamma^4\left(\frac{1}{4}\right)}{48\pi^2} = 0.364739936 \quad (37)$$

We can define  $L_c(b, N)$  at a fixed  $N$  and  $b$  as the length where

$$\Omega(L_c(b, N), b, N) = 0.364739936, \quad (38)$$

and

$$\lim_{N \rightarrow \infty} L_c(b, N) = L_c(b), \quad (39)$$

will be the location of the transition at infinite  $N$ .

Since we are working at a fixed but large  $N$  in this paper, we will define our length scale as

$$a(b) = \frac{1}{L_c(b, N)}. \quad (40)$$

## B. Low lying fermion eigenvalues

The eigenvalues of the massless Hermitian overlap Dirac operator,  $H_o(0)$ , can be used to see how they scale and if they show evidence for chiral symmetry breaking. The eigenvalues come in doubly degenerate pairs and there is also a pairing of positive and negative eigenvalues due to exact chiral symmetry on the lattice. We computed all the eigenvalues of the massless overlap Dirac operator.

Let  $0 < \lambda_k < 1$ ,  $k = 1, \dots, N^2 - 1$  with  $\lambda_k < \lambda_{k+1}$  denote all the positive distinct eigenvalues where each eigenvalue is doubly degenerate and each positive eigenvalue has a negative eigenvalue pair. We can use

$$\lambda(b) = \langle \lambda_1 \rangle \quad (41)$$

as another choice for our length scale.

If chiral symmetry is broken, the chiral condensate sets a scale. In particular, we expect

$$r_k = \left\langle \frac{\lambda_1}{\lambda_k} \right\rangle \quad (42)$$

to be independent of the coupling for a few low values of  $k$ . As  $N$  increases, we expect more  $r_k$  to be independent of the coupling. In addition, we expect  $\lambda(b)$  to approach a finite limit as  $N \rightarrow \infty$ .

## V. SINGLE SITE MODEL WITH MASSLESS ADJOINT FERMIONS

Our choice of  $b$  and  $N$  are based on numerical feasibility. We expect the approach to the large  $N$  limit to get slower as we increase  $b$ . Since the numerical costs increase rapidly with  $N$ , we cannot make  $N$  as large as we wish. Computational costs are manageable if we choose  $N$  in the range of 13 to 25. We will restrict ourselves to mainly a single value of  $N$ , namely,  $N = 18$  and also provide some additional data with  $N = 25$  to understand finite  $N$  effects. We have chosen the couplings in the range  $b \in [0.32, 0.70]$ . Our definition of the coupling is related to the conventional lattice coupling by

$$\beta = 2bN^2. \quad (43)$$

$N$	$b$	$\langle P \rangle$	$a(b)$	$N\lambda(b)$
18	0.32	0.6092(7)	0.4442(24)	0.0544(8)
18	0.35	0.6290(7)	0.4251(23)	0.0507(7)
18	0.40	0.6720(7)	0.3858(22)	0.0440(6)
18	0.45	0.7045(6)	0.3561(29)	0.0381(5)
18	0.50	0.7325(5)	0.3354(27)	0.0330(4)
18	0.53	0.7468(5)	0.3050(36)	0.0301(4)
18	0.55	0.7562(5)	0.2931(29)	0.0279(4)
18	0.57	0.7650(5)	0.2820(28)	0.0278(4)
18	0.60	0.7775(5)	0.2704(26)	0.0256(4)
18	0.65	0.7943(5)	0.2566(29)	0.0229(3)
18	0.70	0.8076(4)	0.2354(131)	0.0213(3)
25	0.40	0.6888(5)	0.3761(27)	0.0404(6)
25	0.45	0.7187(5)	0.3400(34)	0.0362(6)
25	0.50	0.7444(5)	0.3134(18)	0.0318(5)
25	0.55	0.7678(5)	0.2973(17)	0.0277(4)
25	0.60	0.7850(4)	0.2864(15)	0.0238(4)
25	0.65	0.8024(4)	0.2778(17)	0.0218(4)

TABLE I: Table showing the various values of couplings where simulations were performed with massless fermions with  $N = 18$  and  $N = 25$ . The results for the average plaquette and the two different choices for the scales are also shown.

Our range of coupling corresponds to  $\beta \in [2.56, 5.6]$  for SU(2) and  $\beta \in [5.76, 12.6]$  for SU(3). The choice of couplings falls in the range of recent simulations with adjoint fermions using SU(2) as the gauge group [11–13] and also in simulations with fermions in the symmetric two-index representation and SU(3) as the gauge group [15].

In addition to these physical parameters, we also have to choose the value of the Wilson mass parameter,  $m$ , in (11). It is an irrelevant parameter but needs to be chosen in a specific range to realize the correct continuum limit. Based on previous studies on a single site model with adjoint fermions [19], we set  $m = 4$  in this paper.

Table I shows the various values of couplings where simulations were performed along with the results for the average plaquette (c.f. (8)),  $a(b)$  (c.f. (40)), and  $N\lambda(b)$  (c.f. 41)). A plot of the average plaquette is shown in Fig. 1. The plaquette leads off as  $1 - \frac{N-1}{8Nb} + O(b^{-2})$  where the coefficient of  $b^{-1}$  is not affected by fermions. A fit of the data shows a smooth approach to unity as  $b \rightarrow \infty$ . The data also shows a measure of the fact that the eigenvalues of Polyakov loop operators  $U_\mu$  are uniformly distributed. The four data points shown by different colored squares, correspond to the average values of

$$P_\mu = \frac{1}{2} \left( 1 - \frac{1}{N^2} |\text{Tr} U_\mu|^2 \right); \quad (44)$$

for  $\mu = 1, \dots, 4$  with  $P_1 < P_2 < P_3 < P_4$  on every gauge field configuration. An average value of  $\frac{1}{2}$  in the large  $N$  limit shows that the  $Z_N$  symmetries are not broken. Our results are very close to  $\frac{1}{2}$  for both  $N = 18$  and  $N = 25$  and we can assume that reduction to a single site holds and we are simulating an infinite volume theory.

We define

$$b_{\text{tad}} = b\langle P \rangle, \quad (45)$$

as the tadpole improved coupling and plot the running of this coupling versus our two logarithmic scales,  $\ln a(b)$  and  $\ln(N\lambda(b))$  in Fig. 2 and Fig. 3 respectively for the data points listed in Table I. The data with errorbars are shown with solid circles in both figures. We chose one point in the middle of the range as our renormalization point and the solid curve represents the result based on two loop perturbation theory. Clearly, there is no agreement and the coupling runs much faster than what is expected from two loop perturbation theory. This indicates that we are working with lattice couplings that should be considered as strong in spite of the fact that we used values that would be considered as weak in theories that do not have additional fixed points.

We end this section by presenting some details pertaining to the two scales. We plot  $\Omega(L, b, N)$  for  $N = 18$  and  $N = 25$  in Fig. 4. We have set the x-axis to  $L/L_c(b)$  where  $L_c(b)$  is obtained using (38). We see that the value for  $\Omega$  flattens out for large loops and this is a finite  $N$  effect. In addition, it flattens out at a higher value for weaker coupling and this is because finite  $N$  effects sets in at smaller physical loop sizes at weaker coupling. Due to these

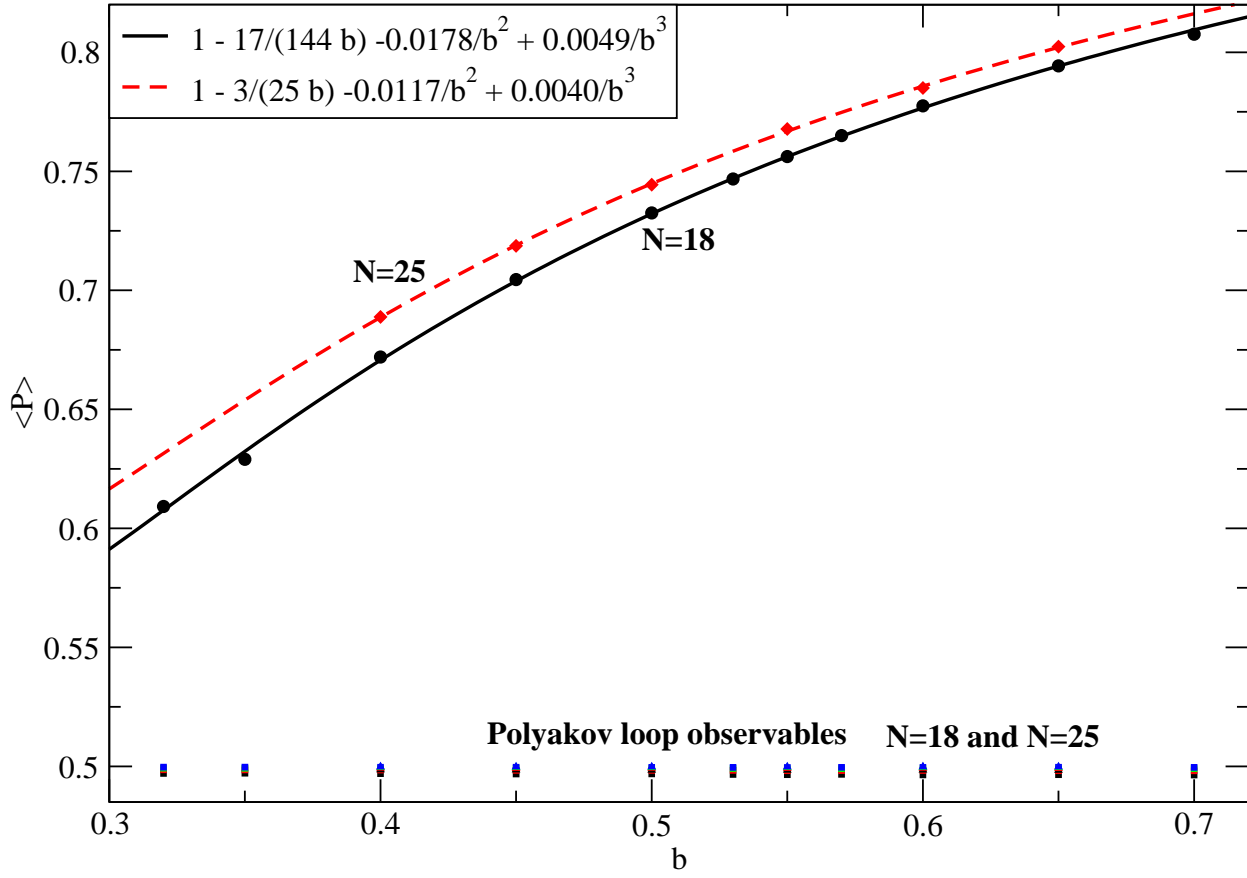


FIG. 1: Average value of the plaquette along with the average values for the four different Polyakov loop observables for massless fermions at  $N = 18$ .

two effects, the determination of  $L_c(b)$  at weaker coupling has larger finite  $N$  effects. We note that the finite  $N$  effect get weaker at  $N = 25$  where we can perform a better estimate of  $L_c(b)$  even at  $b = 0.65$ . The larger finite  $N$  effect at weaker coupling can also be seen in Fig. 2.

The complete spectrum of the distinct eigenvalues of the massless adjoint overlap Dirac operator are shown in Fig. 5 for three different couplings at  $N = 18$  and  $N = 25$ . All three plots show the same qualitative behavior. We see a concentration of small eigenvalues (less than 0.1) followed by a bulk like distribution. We think the distribution for  $\lambda < 0.1$  is due to the would be zero modes in the gauge field background that is diagonal. We believe that this part of the distribution will shows signs of chiral symmetry breaking if one exists. If this is the case, we would expect the lowest eigenvalue to scale like  $\frac{1}{N^2}$ . But we only see evidence for scaling like  $\frac{1}{N}$  in Fig. 3 where a plot with  $\ln(N\lambda(b))$  on the x-axis show good agreement between  $N = 18$  and  $N = 25$ . Therefore, we do not yet see evidence for chiral symmetry breaking.

The plot of  $r_k$  as defined in (42) versus  $k$  is shown in a log-log plot in Fig. 6. Here again, one sees a separation between the low eigenvalues (the would-be zero modes in a diagonal background) and the bulk. Furthermore, the ratios do not change much with coupling for  $k < 5$  for  $N = 18$  and  $k < 7$  for  $N = 25$  showing that the finite  $N$  effect is of order  $\frac{1}{N}$ .



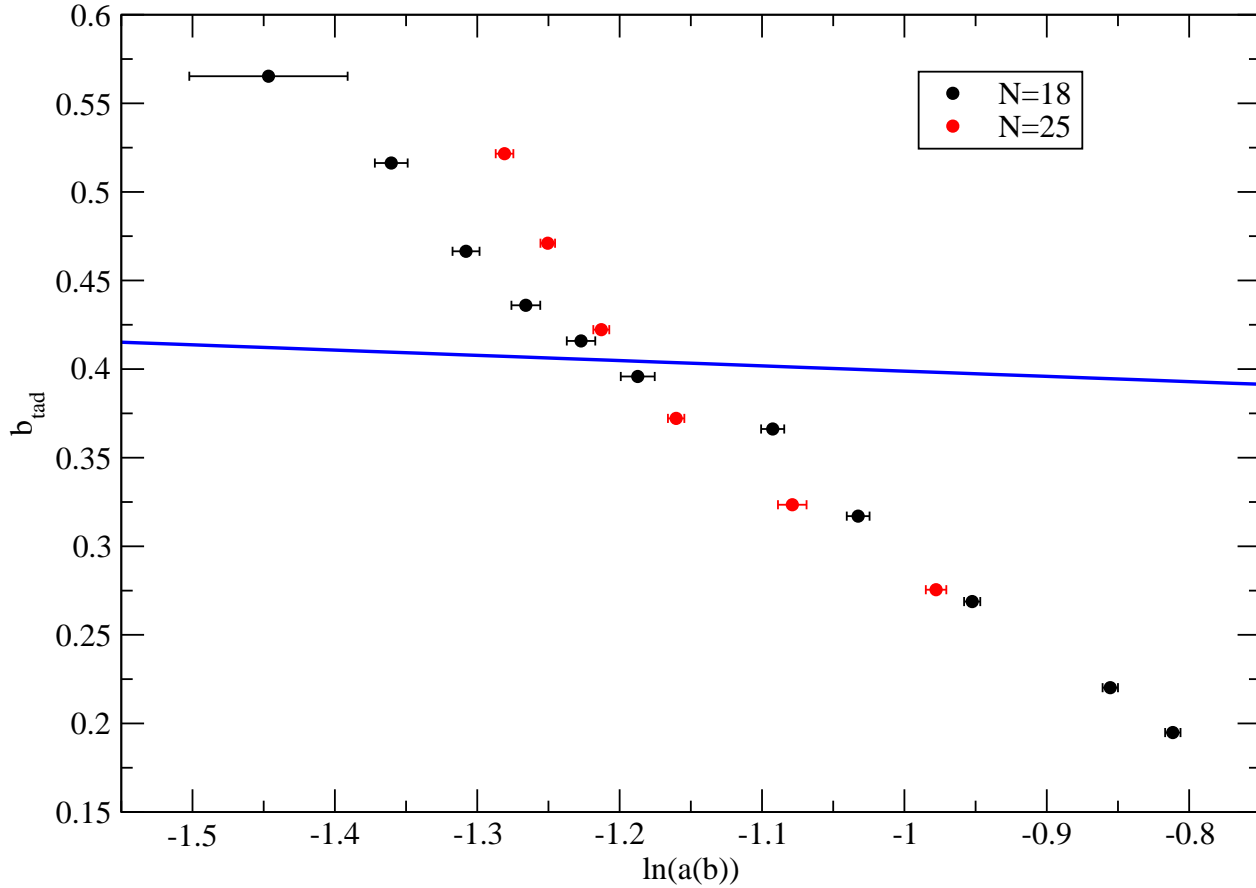


FIG. 2: Running of the tadpole improved coupling versus the logarithmic scale  $\ln a(b)$  for massless fermions at  $N = 18$  and  $N = 25$ .

## VI. SPECULATIONS

How does one see the effect of an infra-red fixed point in a lattice computation? According to the two loop beta function, the zero occurs at

$$b_*(f) = -\frac{b_1}{b_0} = \frac{1}{8\pi^2} \frac{16f - 17}{11 - 4f}. \quad (46)$$

If  $f$  is close to the upper limit of  $\frac{11}{4}$ , the zero occurs at a value of the coupling that can be considered as perturbative. Different choices for  $a(b)$  will not matter in a study of the infra-red fixed point. One should see numerical evidence for a very rapid change of  $a(b)$  versus  $b$  close to  $b_*(f)$  indicative of a zero of the beta function. The critical values for  $f = \frac{3}{2}, 2$  and  $\frac{5}{2}$  are  $b_*(\frac{3}{2}) = \frac{1.4}{8\pi^2}$ ,  $b_*(2) = \frac{5}{8\pi^2}$  respectively.  $b_*(\frac{5}{2}) = \frac{23}{8\pi^2}$ . None of these would be considered perturbative and it is quite likely that the study of the infra-red fixed point is strongly affected by the choice of  $a(b)$ . In particular, it is quite possible that the location of the infra-red fixed point depends on the choice of  $a(b)$  and there is even a possibility that the existence of an infra-red fixed point on either side of the lower boundary of  $f = \frac{17}{16}$  depends on the choice of  $a(b)$ . We have set  $f = 1$  in this study and we clearly do not see perturbative behavior as discussed in Sec. V.

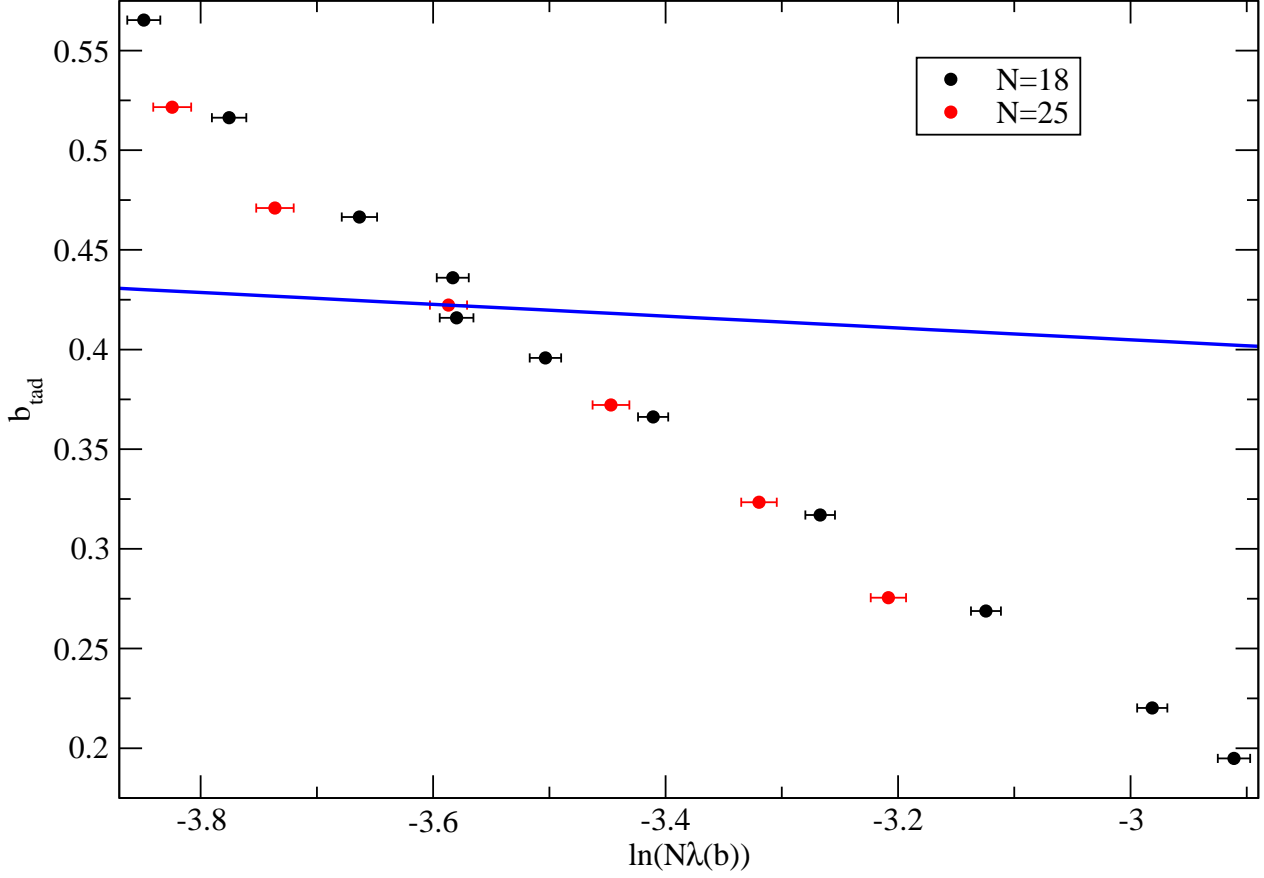


FIG. 3: Running of the tadpole improved coupling versus the logarithmic scale  $\ln \lambda(b)$  for massless fermions at  $N = 18$  and  $N = 25$ .

In order to understand the behavior of the running coupling better, we consider beta functions of the form

$$\begin{aligned}
 \mathbf{A}: \quad \beta(b) &= -b_0 \left(1 - \frac{b_I}{b}\right) \\
 \mathbf{B}: \quad \beta(b) &= -b_0 \left(1 - \frac{b_I}{b}\right) \left(1 - \frac{b_U}{b}\right) \\
 \mathbf{C}: \quad \beta(b) &= -b_0 \left[ \left(1 - \frac{b_*}{b}\right)^2 + \frac{\alpha^2}{b^2} \right] \\
 \mathbf{D}: \quad \beta(b) &= \begin{cases} -b_0 \left|1 - \frac{b_*}{b}\right|^{p+} & \text{for } b > b_* \\ -b_0 s \left|1 - \frac{b_*}{b}\right|^{p-} & \text{for } b < b_* \end{cases}
 \end{aligned} \tag{47}$$

where it is assumed that all parameters except  $s$  are positive and we also assume that  $b_I > b_U$ . The parameter  $s$  could be positive or negative.

- Case **A** is the two loop beta function written for the case where it has a zero.  $b_I$  is the location of the infra-red fixed point. The beta function is shown in solid red in Fig. 7 and the a plot of the coupling with the scale is

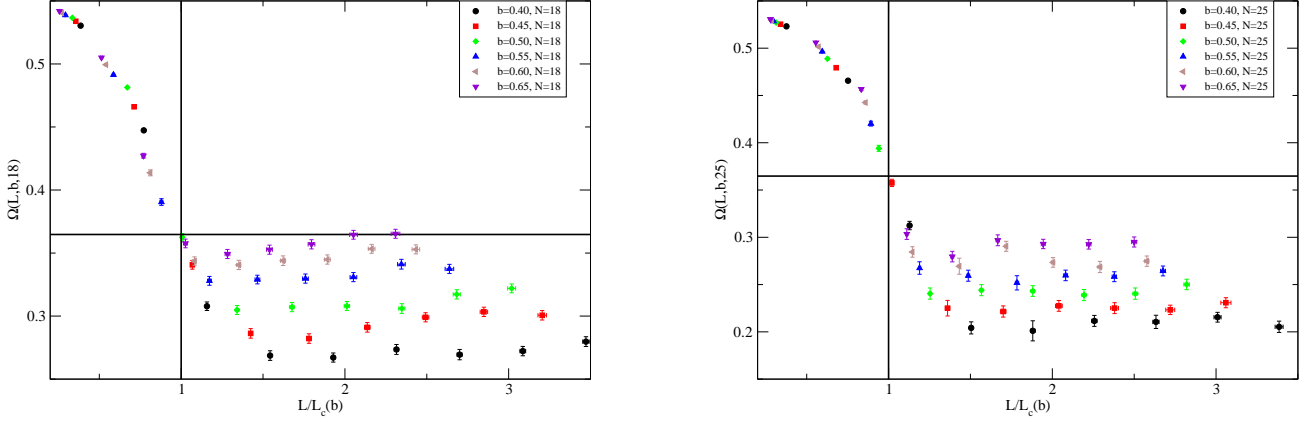


FIG. 4: Plot of the quantity,  $\Omega(L, N, b)$ , as a function of  $L/L_c(b)$  at  $N = 18$  and  $N = 25$  for massless fermions at several different coupling.

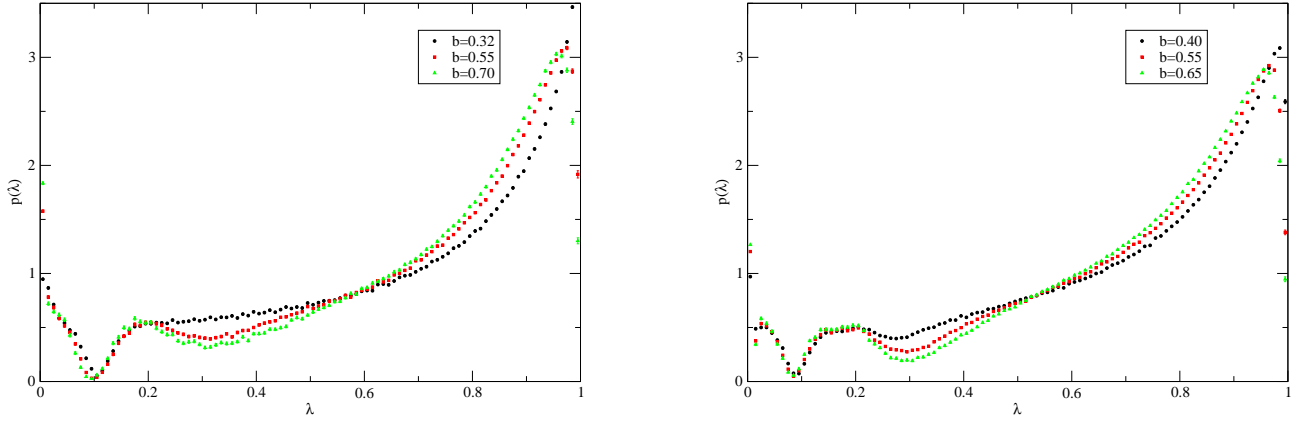


FIG. 5: The full distribution of the eigenvalues of the massless adjoint overlap Dirac operator for three different couplings at  $N = 18$  and  $N = 25$ .

shown in solid red in Fig. 8. The logarithmic scale goes to positive infinity as  $b \rightarrow b_I$ . In order to define the continuum limit, we need to take the limit  $t \rightarrow -\infty$  and this is achieved by taking  $b \rightarrow \infty$  in the usual manner. This is what one expects to see if nothing occurs beyond what is expected in two-loop perturbation theory.

- Cases **B** and **C** have an additional  $\frac{1}{b^2}$  term and were discussed in [27].
  - The beta function and the dependence of coupling on the scale for case **B** are shown in dashed green in Fig. 7 and Fig. 8 respectively. The logarithmic scale goes to positive infinity at  $b = b_I$  and goes to negative infinity at  $b = b_U$  which is an ultra-violet fixed point. In addition to defining a continuum limit as  $b \rightarrow \infty$ , we can also define a continuum theory as  $b \rightarrow b_U$ . It is likely that the location of  $b_U$  depends on the choice of  $a(b)$ . If we assume that a  $b_U$  exists for all choices of  $a(b)$ , then we can define a continuum theory by taking a limit  $b \rightarrow b_U$  that is operator dependent.
  - The case **B** with  $b_I = b_U = b_*$  is same as case **C** with  $\alpha = 0$ . The beta function and the dependence of coupling on the scale for this case are shown in dot-dot-dashed brown in Fig. 7 and Fig. 8 respectively. The limit of  $b \rightarrow b_*$  from above results in the logarithmic scale approaching positive infinity and the limit

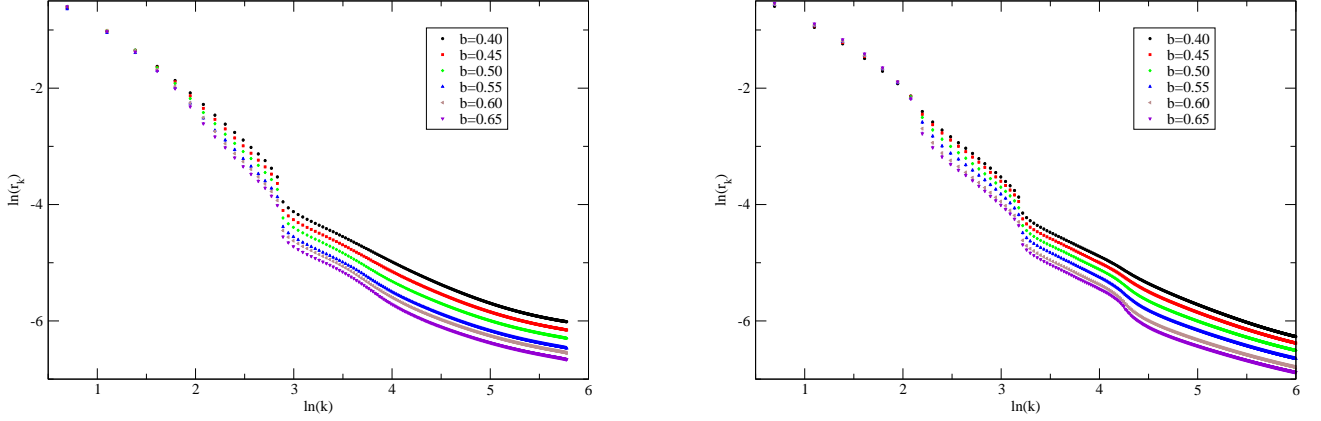


FIG. 6: The ratios of the eigenvalues of the massless adjoint overlap Dirac operator are shown in log-log plot for all couplings common to  $N = 18$  and  $N = 25$  in Table. I.

of  $b \rightarrow b_*$  from below results in the logarithmic scale approaching negative infinity. A continuum theory can be defined in the limit of  $b \rightarrow b_*$  from below. As before,  $b_*$  is expected to depend on the choice of  $a(b)$ .

- The beta function and the dependence of coupling on the scale for case **C** with  $\alpha > 0$  are shown in dot-dashed blue in Fig. 7 and Fig. 8 respectively. In this case, there is a region around  $b = b_*$  where the coupling walks. How far it walks, depends on  $\alpha$  and the range  $[t_I, t_U]$ , where the coupling essentially remains a constant, grows as  $\alpha$  decreases. As before,  $b_*$  is expected to depend on the choice of  $a(b)$ . The continuum limit is defined as  $b \rightarrow \infty$ .
- In all cases discussed above, the location of  $b_I$  and/or  $b_U$  depends on the choice of  $a(b)$ . Case **D** is different in this respect. If the beta function has a zero that is non-analytic, we expect the location of the zero to not depend on  $a(b)$ . In other words, if one observable shows non-analytic behavior at some coupling, all observables are expected to show non-analyticity at the same coupling. If  $s = -1$  and  $p_+ = p_- = 1$ , we recover case **A**. If  $s = 1$  and  $p_+ = p_- = 2$ , we recover case **C** with  $\alpha = 0$ . The beta function and the dependence of coupling on the scale for  $s = 1$  and  $p_+ = p_- = \frac{2}{3}$  are shown in dot-dash-dashed orange in Fig. 7 and Fig. 8 respectively. Like in case **C**, for this choice of parameters, there is a region around  $b = b_*$  where the coupling walks. Whether there is a infra-red/ultra-violet fixed point at  $b = b_*$  depends on the choice of  $p_{\pm}$  as can be seen from Fig. 9.
  - If  $p_- < 1$ , the scale change from  $b = 0$  to  $b = b_*$  is finite. In such a situation, we cannot define a continuum theory by taking  $b \rightarrow b_*$  from below.
  - If  $p_- > 1$ , the logarithmic scale goes to negative infinity as  $b \rightarrow b_*$  from below and  $b_*$  is an ultra-violet fixed point from below. We can define a continuum theory in this limit.
  - if  $p_+ < 1$ , the logarithmic scale starts out at a finite value for  $b = b_*$  and goes down to negative infinity as  $b \rightarrow \infty$ . A continuum theory can be defined as  $b \rightarrow \infty$ .
  - If  $p_+ > 1$ ,  $b = b_*$  is an infra-red fixed point from above and the logarithmic scale goes to positive infinity as  $b \rightarrow b_*$  from above. A continuum theory can be defined as  $b \rightarrow \infty$ .

As the maximum of  $\beta(b)$  moves away from zero in case **C**, the range where the *coupling runs slowly* shrinks. As the power,  $p_{\pm}$ , goes below unity in case **D**, the range where the *coupling runs slowly* shrinks. In such cases, it will be difficult to see evidence for a slow running of the coupling. Instead, one will see a fast running of the coupling on either side of the maximum in case **C** or the location of the singular point in case **D**. The numerical data shown in Fig. 2 and Fig. 3 is close to what is seen in case **C** or case **D** for couplings around  $b_*$ . Since we do not see agreement with perturbation theory and we see a running that is significantly faster, the couplings we are using on the lattice are probably on either side of  $b_*$  and  $f = 1$  probably corresponds to a case where the region of *slow running of coupling* is very small. Clearly, our data is not precise enough to distinguish between either of these cases. But our data suggests the presence of a  $b_*$ .

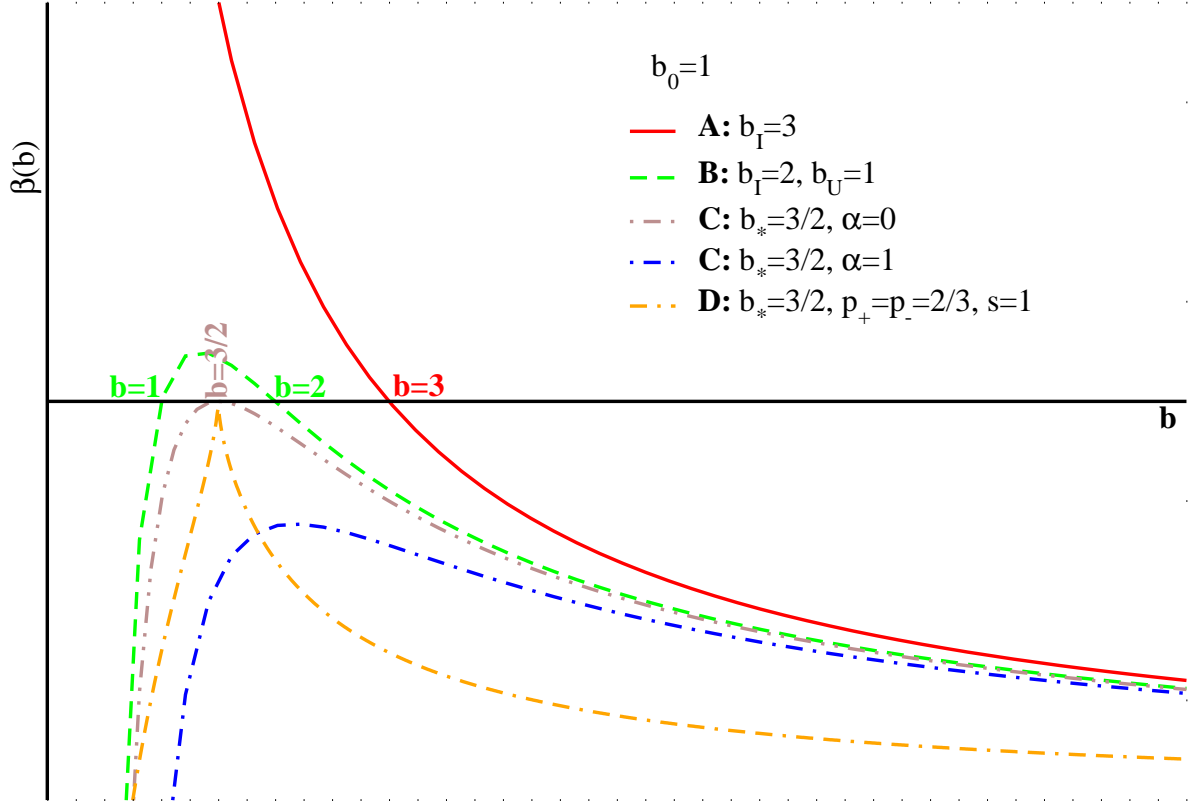


FIG. 7: Different cases for the beta function are shown.

## VII. CONCLUSIONS

The single site model of a large  $N$  gauge theory coupled to massless adjoint fermions was numerically studied in this paper. We have studied this model with a single flavor of adjoint fermion numerically using the Hybrid Monte Carlo algorithm and pseudofermions. We studied the running coupling using two different choice of scales and did not find agreement with two-loop perturbation theory at intermediate values of the tadpole improved coupling. The two different choices of scales were the transition from weak to strong coupling and the lowest eigenvalue of the massless overlap Dirac operator. This is the main result of our paper.

Since one flavor of adjoint fermion is close to  $\frac{17}{16}$  which is the lower bound for the number of flavors for a perturbative zero of the beta function, we speculate on the possibility that a near zero of the beta function might be the cause for our result being not in agreement with perturbation theory. Our numerical data cannot show with definiteness that there is a near-zero of the beta function but the behavior suggests such a possibility.

The results presented in this paper are exploratory in nature and future simulations with different values of  $f$  will give a clearer physics picture. However, the work lays the foundation for the careful study of ultra-violet/infra-red fixed points in matrix models that mimic large  $N$  gauge theories coupled to adjoint fermions. We have the ability to treat the number of fermion flavors as a real number in the matrix model and study the presence of singular behavior in the associated beta function. It is likely that the behavior at the singular point, results in it being an

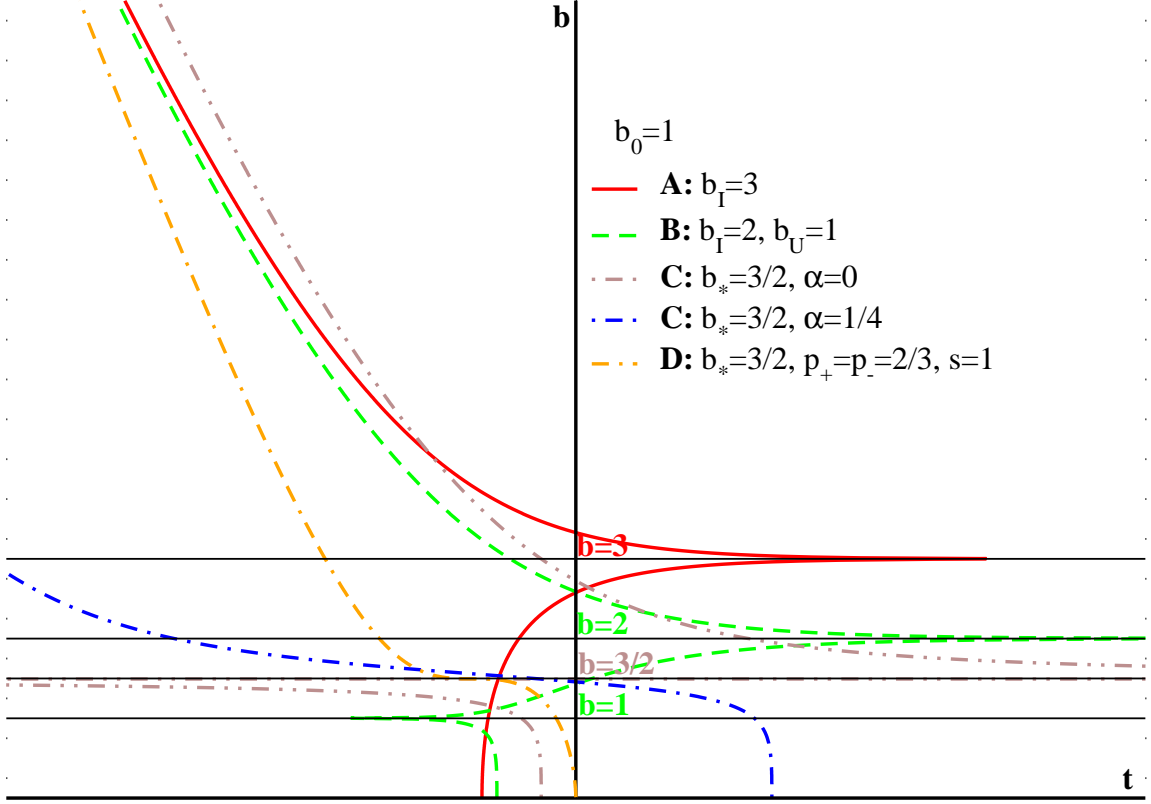


FIG. 8: The running of the coupling with the scale is shown for the different cases of the beta function.

ultra-violet/infra-red fixed point for some range of fermion flavors. The numerical procedure developed in this paper for the case of a single Dirac flavor paves the way for future numerical studies of the matrix model with varying number of flavors.

### Acknowledgments

R.N. acknowledges partial support by the NSF under grant number PHY-0854744. R.N. would like to thank Erich Poppitz for several useful discussions. The numerical calculations presented in this work have been performed on the Horseshoe6 cluster at the University of Southern Denmark (SDU) funded by the Danish Center for Scientific Computing for the project "Origin of Mass" 2009/2010.

---

[1] B. Holdom, Phys. Rev. D **24**, 1441 (1981).

[2] K. Yamawaki, M. Bando and K. -i. Matumoto, Phys. Rev. Lett. **56**, 1335 (1986).

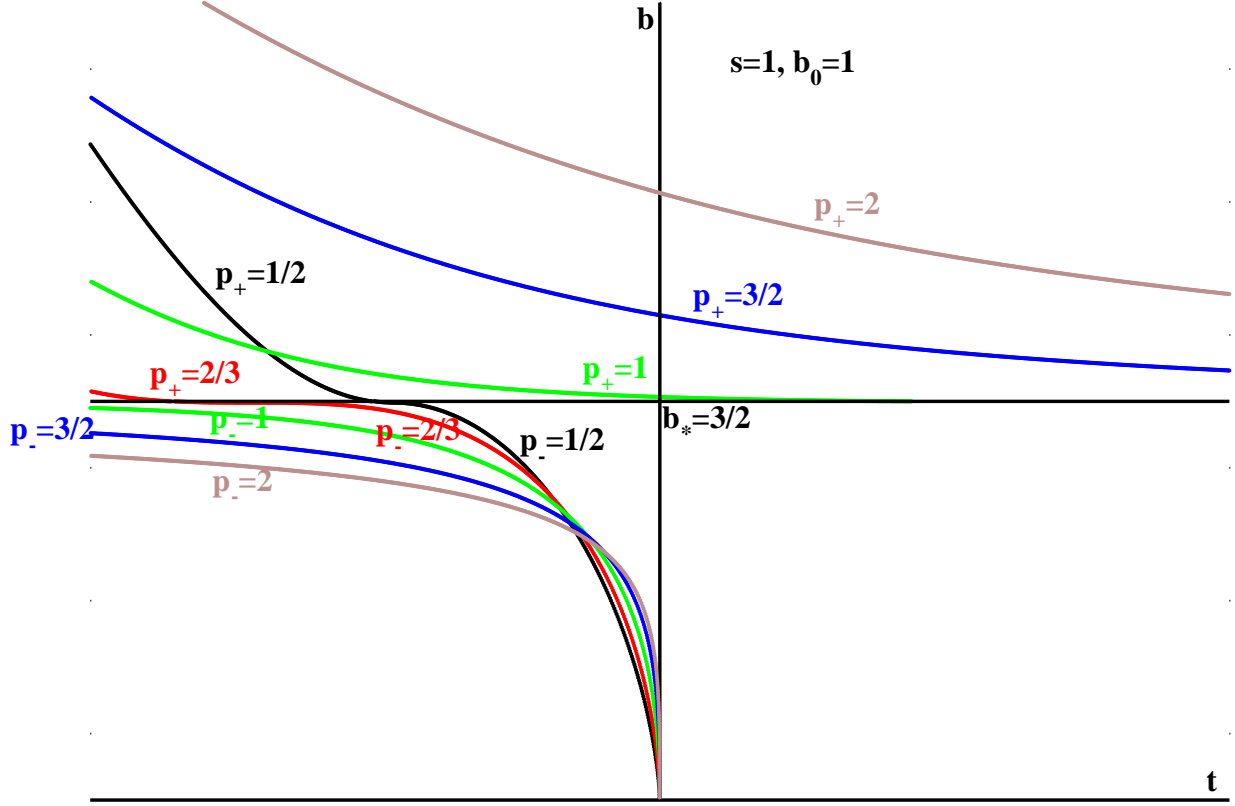


FIG. 9: The running of the coupling with the scale is shown for case **D** with different choices for  $p_{\pm}$  with  $s = 1$  and  $b_0 = 1$ .

- [3] T. W. Appelquist, D. Karabali and L. C. R. Wijewardhana, Phys. Rev. Lett. **57**, 957 (1986).
- [4] J. R. Andersen, O. Antipin, G. Azuelos, L. Del Debbio, E. Del Nobile, S. Di Chiara, T. Hapola, M. Jarvinen *et al.*, [arXiv:1104.1255 [hep-ph]].
- [5] L. Del Debbio, PoS **LATTICE2010**, 004 (2010).
- [6] F. Sannino and K. Tuominen, Phys. Rev. D **71**, 051901 (2005) [hep-ph/0405209]. D. D. Dietrich, F. Sannino, Phys. Rev. **D75**, 085018 (2007). [hep-ph/0611341].
- [7] S. Weinberg, Cambridge, UK: Univ. Pr. (1996) 489 p
- [8] A. Hasenfratz, [arXiv:1106.5293 [hep-lat]].
- [9] T. Appelquist, G. T. Fleming, M. Lin, E. T. Neil, D. A. Schaich, [arXiv:1106.2148 [hep-lat]].
- [10] Z. Fodor, K. Holland, J. Kuti, D. Nogradi, C. Schroeder, Phys. Lett. **B703**, 348-358 (2011). [arXiv:1104.3124 [hep-lat]].
- [11] S. Catterall, L. Del Debbio, J. Giedt, L. Keegan, [arXiv:1108.3794 [hep-ph]].
- [12] T. DeGrand, Y. Shamir, B. Svetitsky, Phys. Rev. **D83**, 074507 (2011). [arXiv:1102.2843 [hep-lat]].
- [13] A. J. Hietanen, K. Rummukainen, K. Tuominen, Phys. Rev. **D80**, 094504 (2009). [arXiv:0904.0864 [hep-lat]].
- [14] F. Bursa, L. Del Debbio, D. Henty, E. Kerrane, B. Lucini, A. Patella, C. Pica and T. Pickup *et al.*, Phys. Rev. D **84**, 034506 (2011) [arXiv:1104.4301 [hep-lat]].
- [15] Y. Shamir, B. Svetitsky, T. DeGrand, Phys. Rev. **D78**, 031502 (2008). [arXiv:0803.1707 [hep-lat]].
- [16] Z. Fodor, K. Holland, J. Kuti, D. Nogradi, C. Schroeder, [arXiv:1103.5998 [hep-lat]].
- [17] J. B. Kogut, D. K. Sinclair, [arXiv:1105.3749 [hep-lat]].

- [18] B. Bringoltz, M. Koren, S. R. Sharpe, [arXiv:1106.5538 [hep-lat]].
- [19] A. Hietanen, R. Narayanan, Phys. Lett. **B698**, 171-174 (2011). [arXiv:1011.2150 [hep-lat]].
- [20] S. Catterall, R. Galvez, M. Unsal, JHEP **1008**, 010 (2010). [arXiv:1006.2469 [hep-lat]].
- [21] T. Azeyanagi, M. Hanada, M. Unsal, R. Yacoby, Phys. Rev. **D82**, 125013 (2010). [arXiv:1006.0717 [hep-th]].
- [22] A. Hietanen, R. Narayanan, JHEP **1001**, 079 (2010). [arXiv:0911.2449 [hep-lat]].
- [23] E. Poppitz, M. Unsal, JHEP **1001**, 098 (2010). [arXiv:0911.0358 [hep-th]].
- [24] B. Bringoltz, JHEP **0906**, 091 (2009). [arXiv:0905.2406 [hep-lat]].
- [25] G. Cossu and M. D'Elia, JHEP **0907**, 048 (2009) [arXiv:0904.1353 [hep-lat]].
- [26] P. Kovtun, M. Unsal, L. G. Yaffe, JHEP **0706**, 019 (2007). [hep-th/0702021 [HEP-TH]].
- [27] D. B. Kaplan, J. -W. Lee, D. T. Son, M. A. Stephanov, Phys. Rev. **D80**, 125005 (2009). [arXiv:0905.4752 [hep-th]].
- [28] R. G. Edwards, U. M. Heller, R. Narayanan, Phys. Rev. **D59**, 094510 (1999). [hep-lat/9811030].
- [29] H. Neuberger, Phys. Lett. **B417**, 141-144 (1998). [hep-lat/9707022].
- [30] R. Narayanan, H. Neuberger, Nucl. Phys. **B443**, 305-385 (1995). [hep-th/9411108].
- [31] R. Narayanan, H. Neuberger, JHEP **0603**, 064 (2006). [hep-th/0601210].
- [32] R. Narayanan, H. Neuberger, JHEP **0712**, 066 (2007). [arXiv:0711.4551 [hep-th]].
- [33] Trivial coefficients of  $N$  get absorbed since we have used the 't Hooft coupling and not  $g^2$ .
- [34] We are assuming that global topology is completely suppressed and one can restrict the theory to the zero topological sector.